Primljen / Received: 18.6.2015.
Ispravljen / Corrected: 10.9.2015.
Prihvaćen / Accepted: 19.9.2015.
Dostupno online / Available online: 10.11.2015.

Numerical model for analysis of stress-ribbon bridges

Authors:

Prof. Jure Radnić, PhD. CE
University of Split
Faculty of Civil Engineering, Arch. and Geodesy
jure.radnic@gradst.hr

Prof.Domagoj Matešan, PhD. CE
University of Split
Faculty of Civil Engineering, Arch. and Geodesy
domagoj.matesan@gradst.hr

Domagoj Buklijaš-Kobojević, MCE
University of Split
Faculty of Civil Engineering, Arch. and Geodesy
domagoj9638@gmail.com

Subject review

Jure Radnić, Domagoj Matešan, Domagoj Buklijaš-Kobojević

Numerical model for analysis of stress-ribbon bridges

A newly developed numerical model for the analysis of stress-ribbon bridges under the short-term (static and dynamic) and long-term loads and actions is presented in the paper. The model can simulate main nonlinear effects of the behaviour of these structures, including nonlinear behaviour of materials, change in the structure geometry, phased construction, prestressing, etc. Basic solutions for the stress-ribbon bridge over the Cetina River near Zadvarje, and some results of its analysis using the developed numerical model, are presented.

Key words:
stress-ribbon bridge, numerical model, static analysis, dynamic analysis, analysis for long-term loading and actions

Pregledni rad

Jure Radnić, Domagoj Matešan, Domagoj Buklijaš-Kobojević

Numerički model za analizu prednapetih provješenih mostova

U radu je prikazan razvijeni numerički model za analizu prednapetih provješenih mostova opterećenih kratkotrajnim statičkim, dinamičkim i dugotrajnim opterećenjima i djelovanjima. Model simulira najvažnije nelinearne efekte ponašanja takvih konstrukcija, uključujući nelinearno ponašanje gradiva, promjene geometrije konstrukcije, nastajanje konstrukcije u fazama, prednapinjanje i sl. Prikazana su osnovna rješenja provješenog mosta preko rijeke Cetine kod Zadvarja, te neki rezultati njegovog proračuna s pomoću razvijenog numeričkog modela.

Ključne riječi:
provješeni most, numerički model, statička analiza, dinamička analiza, analiza za dugotrajno opterećenje i djelovanje

Übersichtsarbeit

Jure Radnić, Domagoj Matešan, Domagoj Buklijaš-Kobojević

Numerisches Model zur Analyse von Spannbandbrücken

In dieser Arbeit wird ein numerisches Model dargestellt, das zur Analyse von Spannbandbrücken unter kurzfristigen statischen und dynamischen sowie unter langfristigen Lasten und Einwirkungen entwickelt wurde. Das Model simuliert die wichtigsten nichtlinearen Effekte des Verhaltens solcher Konstruktionen, einschließlich des nichtlinearen Materialverhaltens, der Veränderungen geometrischer Abmessungen, der einzelnen Entstehungsphasen des Tragwerks, des Vorspannens etc. Dabei sind die wichtigsten Lösungsvarianten der Spannbandbrücke über den Fluss Cetina bei Zadvarje dargestellt und auf dem entwickelten numerischen Model beruhende Resultate entsprechender Berechnungen erläutert.

Schlüsselwörter:
Spannbandbrücke, numerisches Model, statische Analyse, dynamische Analyse, Analyse für langzeitige Lasten und Einwirkungen

1. Introduction

Tension ribbon bridges, or the so called stress-ribbon bridges, rank among the oldest types of bridges. In such bridges, the superstructure (catenary) also assumes the role of the pavement structure. The construction of modern bridges with such load bearing systems started in the mid 1970s. According to the superstructure solution used, these bridges can generally be classified into two groups. The first group includes simple structural solutions with two tendons or steel catenaries supporting the deck slab. These systems exhibit a small flexural stiffness and great deformability, and are highly sensitive to dynamic loading. The second group involves modern solutions in which load-bearing tendons lie within the prestressed reinforced-concrete deck slab, with which they are linked either continuously or at specified points. Such systems are characterised by lower flexural and torsional stiffness, and are less sensitive to deformations and dynamic loads.

The usual deflection (f) to span (L) ratio of stress-ribbon bridges is f/L = 0,02 to 0,03 (Figure 1). To take into account the serviceability requirements, the maximum longitudinal grade of stress-ribbon bridges is in most cases taken to be 12 %. Most existing stress-ribbon bridges are destined for the pedestrian-bicycle traffic only. This is due to a significant change in bridge grade above the supports, and to problems with excessive displacements and vibrations during passage of heavy vehicles. The basic advantage of stress-ribbon bridges is their rationality, rapid semi-prefabricated construction, favourable appearance, minimum depth of the span structure, harmonious blending with the surrounding natural environment, rational maintenance, and minimum impact to environment during construction. Drawbacks of such bridges are namely their high deformability, sensitivity to vibrations, and considerable horizontal forces acting on abutments.

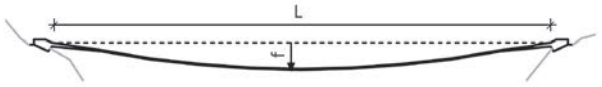

Figure 1. Typical stress-ribbon bridge

Due to their specific features and small number compared to other existing bridges, very few experts are currently involved in the design and realisation of stress-ribbon bridges. The idea for the first modern concrete stress-ribbon bridge was presented in 1958 by the well known German engineer Urlich Finsterwalder as a solution for the bridge over the Bosporus. Jiri Strasky [1], the greatest designer and builder of stress-ribbon bridges, developed in the late twentieth century a successful semi-prefabricated construction procedure for such bridges, involving the following construction stages:

- substructure construction,
- tensioning of load-bearing tendons,
- assembly of prefabricated concrete slabs and prestressed tendons, and placing of additional traditional deck slab reinforcement,
- monolithisation of semi-prefabricated deck slab elements,
- tensioning of tendons and grouting (Figure 2).

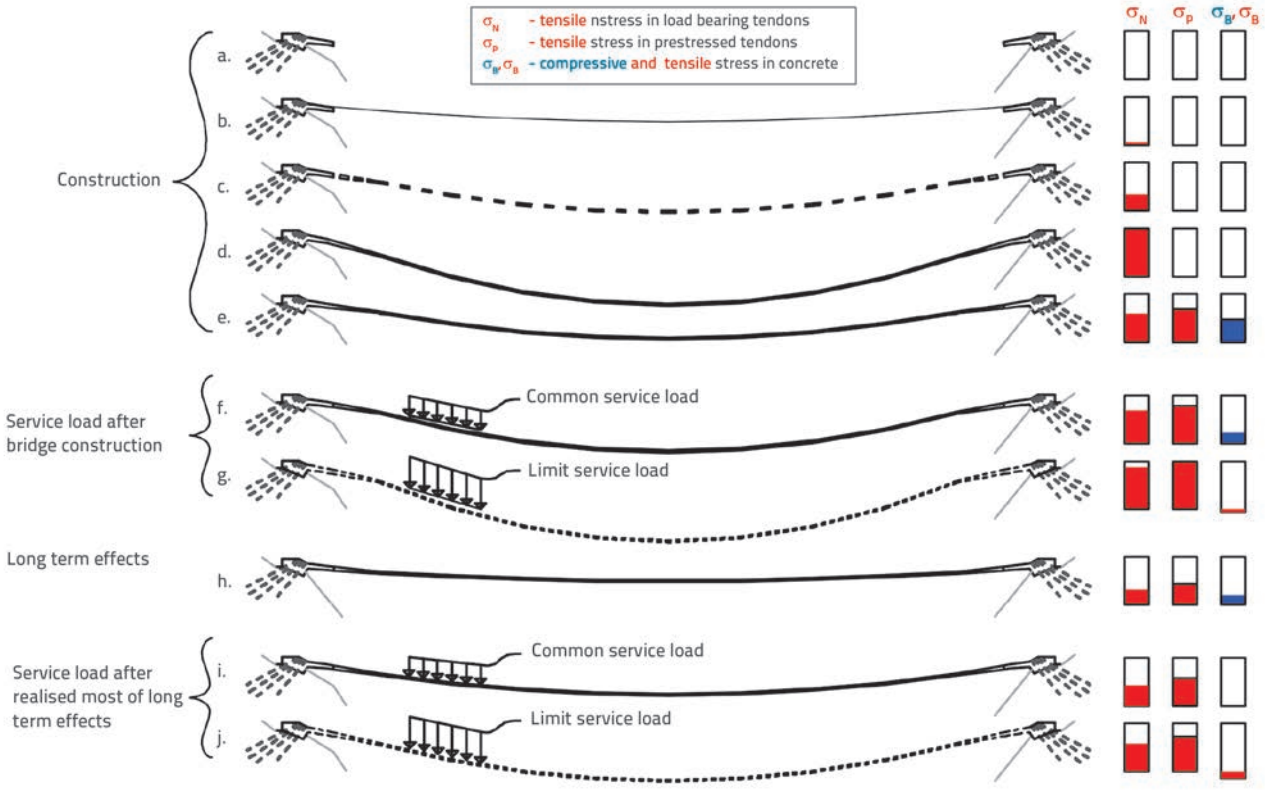

Figure 2. Realization phases and stress change in load-bearing structure of bridge

During construction of a stress-ribbon bridge, its cross section and load-bearing system changes and, over time, the stress in concrete, traditional reinforcement, and tendons, also changes due to rheological effects of concrete (Figure 2). At the superstructure realization stage, the entire weight of prestressed concrete slabs, in situ concrete, reinforcement, and tendons, is assumed by load-bearing tendons acting as pure catenaries. The catenary deflection decreases with an increase in its initial sag (f) and with reduction of the permanent load.

The stiffness and bearing capacity of the superstructure increase after hardening of the in situ concrete and tensioning of prestressed tendons. The bridge level lifts (the sag reduces) and the force level in load-bearing tendons decreases during the prestressed tendon tensioning process. The prestressing can be conducted in phases provided that the first phase is conducted as soon as practicable so as to reduce cracking due to shrinkage and wind load. After the final prestressing, the concrete has to have a sufficient compressive prestress so as to avoid occurrence of tension (concrete cracking) at service load. Cracks in the superstructure can however be expected at limit states, especially at connection to the abutments. This part of the bridge is subjected to high stresses, and so a particular attention must be paid to its shaping and calculation. In fact, the bridge behaviour next to supports is closer to cantilever behaviour, while it is closer to catenary behaviour in zones close to the centre of the bridge. Crack widths next to supports are controlled by adequate support selection, careful shaping, adequate reinforcement details, favourable guidance of tendons, etc. Some possible superstructure shaping alternatives can be found in [1].

Over time, shrinkage and creep occur in concrete, while relaxation of stress occurs in tendons. The bridge sag is reduced due to concrete creep. The entire process results in the decrease of the total prestressing force, and in redistribution of stress in the concrete, traditional reinforcement, prestressed tendons, and load-bearing tendons. As a very young in situ concrete is pretensioned (concrete in prefabricated concrete slabs is older), the influence of concrete creep is significant. Because the creep of in situ concrete is greater than that of prefabricated concrete, the former transfers a part of its initial stress to the prefabricated concrete and traditional reinforcement. The force drops in prestressed and load bearing tendons due to their shortening resulting from the reduced sag of the bridge. Because of force drop in load-bearing tendons, prestressed tendons take on a part of the bridge's weight from the load-bearing tendons.

A significant problem with stress-ribbon bridges are their excessive vibrations and displacements, caused by traffic load and wind. A stress-ribbon bridge can be stabilised by changing the stiffness to bridge mass ratio, by increasing the superstructure mass, and by increasing damping during vibration of the bridge (by installing dampers, adequate structural details, etc.). The global load-bearing system of the bridge is closest to catenary in vertical plane, while in horizontal plane it is closest to the thin-walled girder peripherally restrained on both sides. Due to small superstructure thickness, stress-ribbon bridges exhibit a small flexural stiffness in vertical plane. This results in significant displacements when a point load is transferred along the bridge (group of people or a heavy load). Bridges must also exhibit a sufficient stiffness in horizontal plane. In fact, the torsional and horizontal flexural stiffness of the bridge directly influence its swinging and buckling. Greater superstructure stiffness is achieved by increasing the bridge width and by strengthening the deck slab cross section edges and, in case of larger spans, by installing additional external tendons. It is recommended to keep torsional and horizontal (swinging) vibration modes sufficiently away from the first vertical modes, so as to prevent their superposition. It is also recommended to keep the first vibration modes outside of the walking step period. Although this last requirement is seldom respected, many bridge examples show that the mass and internal damping are quite sufficient for their stabilisation with regard to vibrations. To reduce problems related to vibrations and aerodynamic stability of stress-ribbon bridges, favourable aerodynamic bridge cross-section shapes are nowadays used, and bridge behaviour is tested in wind tunnels. Unfortunately, no modern stress-ribbon bridge has so far been built in Croatia.

In order to provide for considerable deformability of stress-ribbon bridges, the issue of geometric nonlinearity (large displacements) must be taken into account during their design. Many commercial software for the design of these bridges are now available. However, just a few of them are capable of modelling their actual behaviour under the short term (static and dynamic) and long-term loads and actions. One of the models for preliminary design of stress-ribbon bridges is presented in [2]. Regulations for the design and calculation of stress-ribbon bridges are so far available in Japan only [3]. Some research and investigations related to these bridges are given in [4-8].

This paper first presents a nonlinear numerical model that has been developed for the analysis of stress-ribbon bridges subjected to short-term and long-term loads and actions. The model can accurately simulate main nonlinear effects of the bridges under the mentioned loads and actions, including the influence of the change in the structure geometry, prestressing, structure forming in stages, rheological properties of concrete, tensioned steel relaxation, etc. The paper then briefly presents main design solutions for the planned stress-ribbon bridge over the Cetina canyon near Zadvarje, as well as some results of its analysis using the described numerical model. Main conclusions are presented in the final part of the paper.

2. Developed numerical model

2.1. General

The models relevant for the analysis of stress-ribbon bridges subjected to short and long-term loads and actions, which are capable of accurately describing their real behaviour under service conditions and at failure, must adequately model at least the following:

- spatial geometry of the load-bearing system and its stiffness,
- main nonlinear effects of all materials,
- change in the structure's geometry under load (large displacements),

- change in the cross-section and bearing system of the bridge during construction, i.e. staged realization of the structure,
- prestressing,
- rheological effects in concrete (creep, shrinkage, ageing) and prestressed steel (prestressing force losses).

The developed numerical model for the analysis of stress-ribbon bridges that can simulate all of the above mentioned effects is briefly described below. The model is a compilation and upgrade of the previously developed numerical models for the static and dynamic analysis of structures and for the analysis of structures under a long-term load [9-17]. The model upgrade consists in its capability to model stages construction of structures, in a more accurate modelling of shear failure of concrete, and in more efficient calculation procedures.

2.2. Spatial discretisation

The finite element method is used for the spatial discretisation of structure. The tension ribbon is modelled by the element of a thin degenerated shell, which describes its behaviour quite accurately. 8- and 9- node elements are used, with the layered material modelling across the shell thickness (Figure 3). The reinforcing steel is modelled as a separate layer of an appropriate thickness, with the strength and stiffness presented in the bar direction only [9-11].
By spatial discretisation and using the finite element method, the dynamic structural equilibrium equation can be written as follows

$$\mathbf{M}\,\ddot{\mathbf{u}} + \mathbf{C}(\dot{\mathbf{u}}) + \mathbf{R}(\mathbf{u}) = \mathbf{f} \tag{1}$$

where **u** are unknown node displacements, $\dot{\mathbf{u}}$ are velocities and $\ddot{\mathbf{u}}$ are accelerations; **M** is the mass matrix, **C** is the damping matrix and **R(u)** is the vector of internal forces; **f** is the vector of external node forces that can be generated by the wind, machines, etc. ($\mathbf{f} = \mathbf{F}(t)$) or by earthquake ($\mathbf{f} = \mathbf{M}\ddot{\mathbf{d}}_0(t)$). At that, $\ddot{\mathbf{d}}_0$ is the ground acceleration vector, and *t* is the time. The vector of internal forces **R(u)** can be written as follows:

$$\mathbf{R}(\mathbf{u}) = \mathbf{K}\mathbf{u}; \quad \mathbf{K} = \partial\mathbf{R} / \partial\mathbf{u} \tag{2}$$

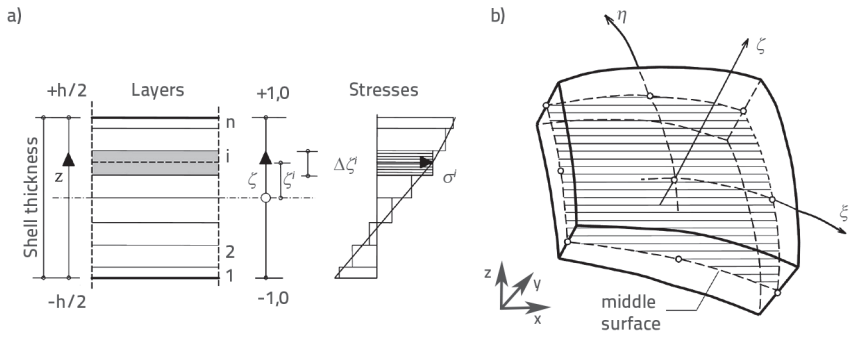

Figure 3. Finite shell element concept: a) layered model across the shell depth; b) degenerated three-dimensional shell element

where **K** is the structural stiffness matrix.
In order to solve of the problem, equation (1) is reduced to:

$$\mathbf{K}\mathbf{x} = \lambda\mathbf{x} \tag{3}$$

where **x** is the characteristic vector and λ is the characteristic value (eigenvalue). For static problems, (1) is reduced to

$$\mathbf{R}(\mathbf{u}) = \mathbf{K}\mathbf{u} = \mathbf{f} \tag{4}$$

where **f** is the external static load.

2.3. Time discretisation

The implicit Newmark algorithm, developed in its iterative form by Hughes [18], is used for solving equation (1). The equilibrium equation requirements are satisfied in time $t_{n+1}=t_n+\Delta t$, i.e. in the $(n+1)$ time increment [9-11].

$$\mathbf{M}\,\ddot{\mathbf{u}}_{n+1} + \mathbf{R}(\mathbf{u}_{n+1}, \dot{\mathbf{u}}_{n+1}) = \mathbf{f}_{n+1} \tag{5}$$

where

$$\begin{aligned} \mathbf{u}_{n+1} &= \bar{\mathbf{u}}_{n+1} + \beta\Delta t^2\ddot{\mathbf{u}}_n \\ \dot{\mathbf{u}}_{n+1} &= \bar{\dot{\mathbf{u}}}_{n+1} + \gamma\,\Delta t\,\ddot{\mathbf{u}}_n \end{aligned} \tag{6}$$

$$\begin{aligned} \bar{\mathbf{u}}_{n+1} &= \mathbf{u}_n + \Delta t\,\dot{\mathbf{u}}_n + 0{,}5(1-2\beta)\Delta t^2\ddot{\mathbf{u}}_n \\ \bar{\dot{\mathbf{u}}}_{n+1} &= \dot{\mathbf{u}}_n + (1-\gamma)\,\Delta t\,\ddot{\mathbf{u}}_n \end{aligned} \tag{7}$$

In the above expressions, Δt is the time step, and n is the time increment; $\bar{\mathbf{u}}_{n+1}$ and $\bar{\dot{\mathbf{u}}}_{n+1}$ are assumed displacement and velocity values, and $\mathbf{u}_{n+1}$ and $\dot{\mathbf{u}}_{n+1}$ are their corrected values; β and γ are the parameters determining the stability and accuracy of the method. By inserting (6) and (7) into (5), and by introducing the incremental-iterative procedure for general nonlinear problem solving, the so called effective static problem is obtained:

$$\mathbf{K}^*_\tau\Delta\mathbf{u} = (\mathbf{f}^*)^i \tag{8}$$

where the effective tangent stiffness matrix $\mathbf{K}^*_\tau$ is calculated in time t using

$$\mathbf{K}^*_\tau = \frac{\mathbf{M}}{\beta\Delta t^2} + \gamma\frac{\mathbf{C}_\tau}{\beta\Delta t} + \mathbf{K}_\tau \tag{9}$$

and the effective load vector $\mathbf{f}^*$ using

$$\mathbf{f}^* = \mathbf{f}_{n+1} - \mathbf{M}\ddot{\mathbf{u}}^i_{n+1} - \mathbf{R}(\mathbf{u}^i_{n+1}, \dot{\mathbf{u}}^i_{n+1}) \tag{10}$$

In the above expressions, n denotes the time step, and i the iteration step; Δ**u** is the displacement increase vector. The implicit Newmark algorithm for iterative problem solving is presented in Table 1.

Table 1. Implicit Newmark algorithm for iterative problem solving

(1)	For the time step (n+1), add the iteration step i = 1
(2)	Calculate vectors for assumed displacements, velocities, and acceleration at the beginning of the time step, using known values from the previous time step: $\mathbf{u}_{n+1}^{1} = \bar{\mathbf{u}}_{n+1} \qquad \dot{\mathbf{u}}_{n+1}^{1} = \bar{\dot{\mathbf{u}}}_{n+1} \qquad \ddot{\mathbf{u}}_{n+1}^{1} = \left(\mathbf{u}_{n+1}^{1} - \bar{\mathbf{u}}_{n+1}\right) \Big/ \left(\beta\, \Delta t^2\right)$
(3)	Calculate effective residual forces $\left(\mathbf{f}^*\right)^i$: $\left(\mathbf{f}^*\right)^i = \mathbf{f}_{n+1} - \mathbf{M}\ddot{\mathbf{u}}_{n+1}^{i} - \mathbf{U}\left(\mathbf{u}_{n+1}^{i}, \dot{\mathbf{u}}_{n+1}^{i}\right)$
(4)	Calculate the effective stiffness matrix $\mathbf{K}_\tau^*$ (if necessary): $\mathbf{K}_\tau^* = \frac{\mathbf{M}}{\beta \Delta t^2} + \gamma \frac{\mathbf{C}_\tau}{\beta \Delta t} + \mathbf{K}_\tau$
(5)	Calculate the displacement increment vector $\Delta\mathbf{u}$: $\mathbf{K}_\tau^* \Delta\mathbf{u}^i = \left(\mathbf{f}^*\right)^i$
(6)	Correct assumed displacement, velocity, and acceleration values: $\mathbf{u}_{n+1}^{i+1} = \mathbf{u}_{n+1}^{i} + \Delta\mathbf{u}_{n+1}^{i} \qquad \ddot{\mathbf{u}}_{n+1}^{i+1} = \left(\mathbf{u}_{n+1}^{i+1} - \bar{\mathbf{u}}_{n+1}\right) \Big/ \left(\beta\, \Delta t^2\right) \qquad \dot{\mathbf{u}}_{n+1}^{i+1} = \dot{\mathbf{u}}_{n+1}^{i} + \left(\gamma\, \Delta t\right)\, \ddot{\mathbf{u}}_{n+1}^{i+1}$
(7)	Control convergency of the process: If $\Delta\mathbf{u}^1$ meets the convergency criterion: $\left\|\Delta\mathbf{u}^i\right\| \Big/ \left\|\mathbf{u}_{n+1}^{i+1}\right\| \le \varepsilon_n$ pass on to the next time step ("n" is replaced with "n+1" and then pass on to the solution step (1)). The solution in time t_{n+1} is: $\mathbf{u}_{n+1} = \mathbf{u}_{n+1}^{i+1} \qquad \dot{\mathbf{u}}_{n+1} = \dot{\mathbf{u}}_{n+1}^{i+1} \qquad \ddot{\mathbf{u}}_{n+1} = \ddot{\mathbf{u}}_{n+1}^{i+1}$ If the convergency criterion is not satisfied, the iteration procedure with correction of displacement, velocity and acceleration values is continued ("i" is replaced with "i+1", and the operation continues with the solution step (3)).

2.4. Modelling change in structure geometry

The change in structure geometry is determined using the so called updated Lagrangian procedure that is based on the following assumptions [11]:

- External load is applied in increments. An iterative calculation procedure is applied for each increment until the unbalanced force vector is sufficiently small. Once the convergence criterion is satisfied, the unbalanced force vector is added to the next external load increment and the iteration procedure is resumed.
- The traditional Lagrange procedure is used in each iteration step: the state of variables is defined as related to the state at the beginning of the iteration procedure.
- At the end of each iteration step, the state of variables is updated (redefined) as related to the state at the end of the iteration step considered.

The geometric nonlinearity model with large displacements and small deformations is included. As previously stated, the influence of large displacements is covered with transformations of displacement and force (stress) components between the global and local coordinate system. In fact, assuming that the increase in displacement within each iteration step is small, it can be stated that there is a linear dependence between deformation and displacement. This greatly simplifies and reduces the calculation procedure. The use of the local coordinate system for defining the constitutive material model also simplifies the analysis for the cases when materials exhibit anisotropic properties.

2.5. Material model for short-term static load

2.5.1. Model for concrete

A very simple concrete model based on its basic parameters is used [9-11] (uniaxial compressive and tensile strength, elastic modulus and Poisson ratio). A graphical interpretation of the model is given in Figure 4.

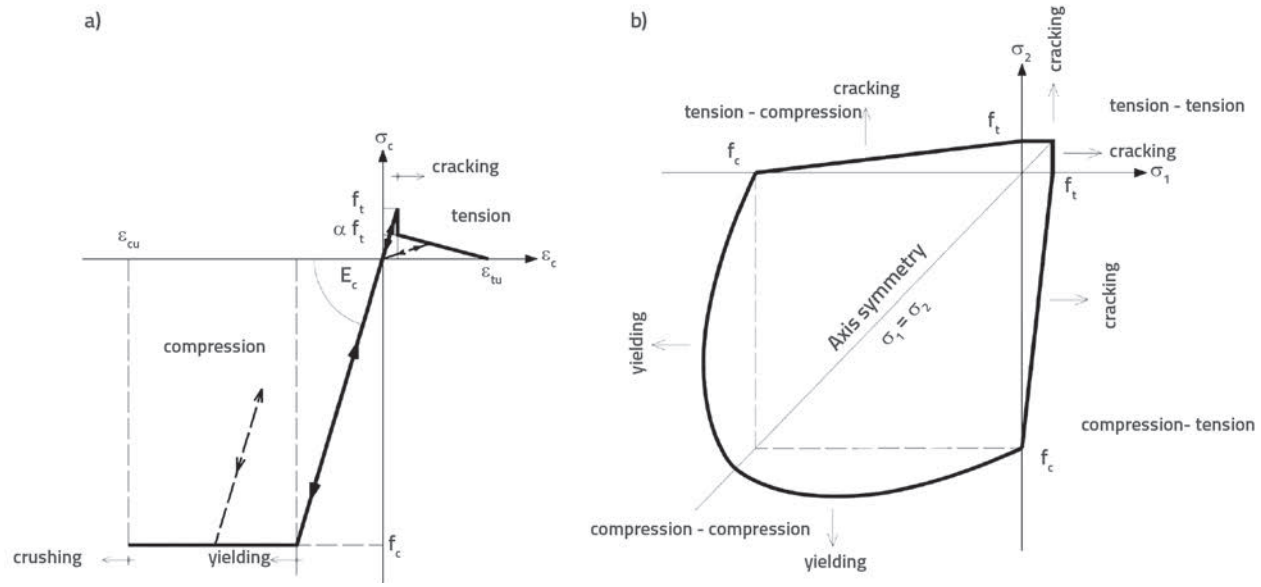

Figure 4. Graphical representation of the adopted concrete model: a) one-dimensional presentation; b) 2D presentation in the field of principal stresses

Modelling of concrete in tension

The linear-elastic behaviour of concrete is assumed until its tensile strength is reached. It is assumed that cracks can occur only in planes that are perpendicular to the mean plane of the shell. It is assumed that each concrete segment is in the state of plane stress. A model of smeared cracks is adopted, i.e. it is assumed that concrete remains in continuum even after cracking. The so called fixed orthogonal cracks model is used. The partial and full closure of cracks in unloading is modelled, as well as the reopening of previous cracks due to repeated load. The contribution of tensile stiffness of uncracked concrete between cracks is simulated in a usual manner, i.e. indirectly by the "descending curve" of the σ - ε diagram for concrete in tension. The simulation of shear stiffness of cracked concrete (the effect of aggregate interlock and friction between the crack plains) is modelled by reducing the shear modulus (G_{12}, G_{13}, G_{23}) depending on the strain, perpendicular to the crack plane.

Modelling of concrete in compression

The theory of plasticity is used for modelling concrete behaviour in compression. The linear-elastic behaviour of concrete is assumed in the beginning of the loading process, until the yield condition is satisfied. After that, the plastic behaviour of concrete is assumed. The so called associated flow is used, i.e. the normality of the plastic deformation vector with regard to yield surface is assumed. The criterion of concrete crushing in

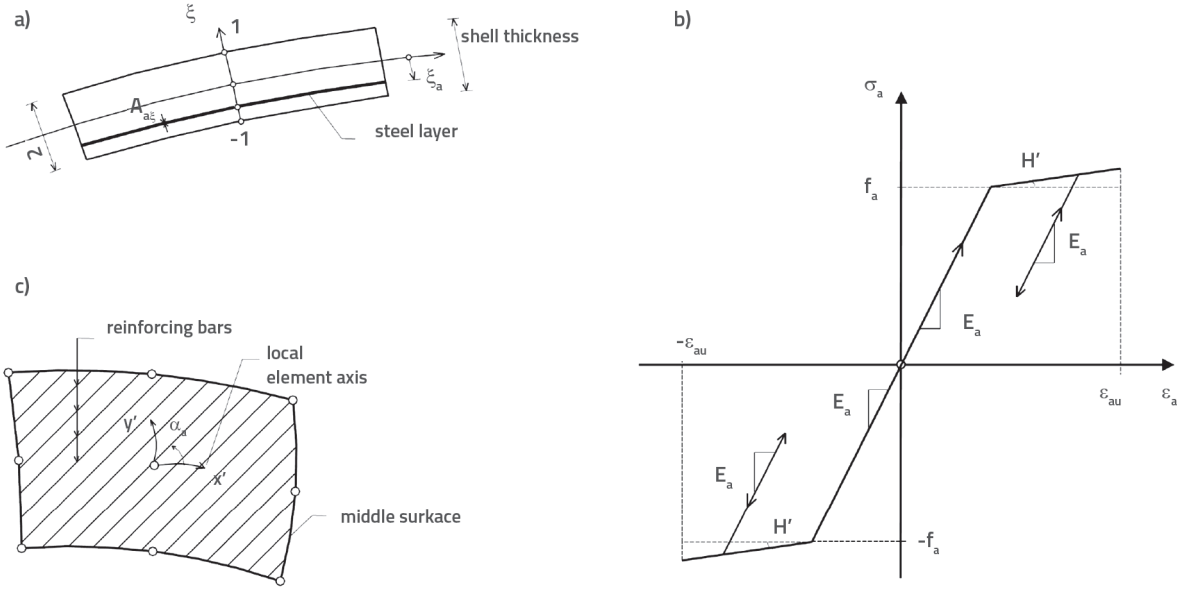

Figure 5. Reinforcement modelling: a) reinforcement layer; b) s-e relationship for steel; c) spreading of reinforcing bars

compression is defined through strain components. The elastic behaviour is assumed in unloading. No concrete stiffness is adopted after concrete crushing.

2.5.2. Reinforcement model

The reinforcement modelling method [9-11] is graphically presented in Figure 5. Reinforcing bars are modelled as separate steel layer of equivalent (normalised) thickness, spaced at an appropriate (normalised) distance from the central plane of the shell. The stress can occur only in the bar direction. A full compatibility between the reinforcement displacement and the surrounding concrete was assumed (no bar slipping possibility). The steel behaviour is described using the bi-linear σ - ε relationship, equally for compression and tension. An elastic behaviour was assumed in unloading, with an initial elastic modulus. Bar failure occurs when the strain in the direction of their spreading exceeds the specified limit value.

2.6. Material model for dynamic load

The material models described in section 2.4, extended to include effect of strain rate on the concrete and steel behaviour, is used to analyse of structure under dynamic load. The model, briefly described below, is presented in detail in [17].

2.6.1. Concrete model

The adopted model, presented in Figure 6, covers a simple dependence of compressive and tensile strength (representing the yield surfaces), and the initial elastic modulus of concrete as related to the equivalent concrete strain rate. In the scope of the numerical procedure, the equivalent strain rate $\dot{\varepsilon}$ is calculated in each time step of the respective time domain as follows:

$$\dot{\varepsilon} = \left\{ \left[2\left(\dot{\varepsilon}_{xx}^2 + \dot{\varepsilon}_{yy}^2 + \dot{\varepsilon}_{zz}^2\right) + \dot{\varepsilon}_{xy}^2 \right] / 3 \right\}^{1/2} \quad (11)$$

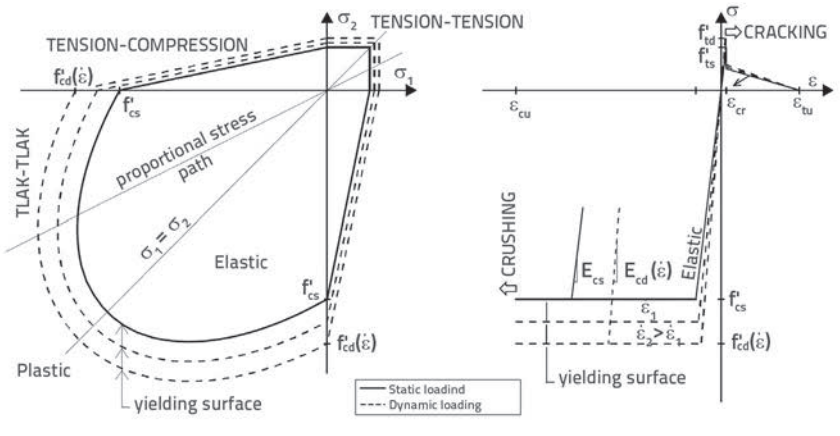

Figure 6. Graphical presentation of concrete model under dynamic load conditions: a) presentation in the field of principal stress values; b) one-dimensional presentation

Current compressive and tensile strength values and elastic modulus values for concrete are calculated, as related to $\dot{\varepsilon}$, in each integration point of each element. The same dependence of mechanical properties of concrete on the strain rate is adopted for all concrete types. The limit (failure) strain of concrete and the Poisson ratio are adopted as fixed values, i.e. as values independent from the concrete strain rate. Reduction of concrete strength at repeated load is not taken into account.

2.6.2. Reinforcement model

A schematic presentation of the steel model is given in Figure 7. The yield limit is not fixed, i.e. it is dependent on the steel elastic strain rate $\dot{\varepsilon}_e$ (in the bar spreading direction). The relationship between the dynamic f_{ad} and static f_{as} yield limit (strength) is assumed to be the same for all steel types. It is assumed that the modulus of elasticity and failure strain of steel are fixed values, i.e. values that are independent from strain rate.

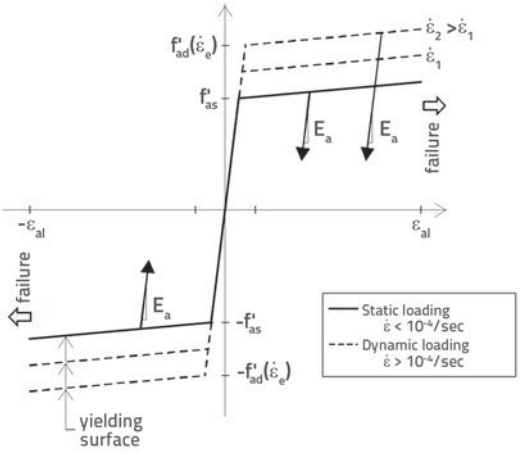

Figure 7. Graphical presentation of steel model under dynamic load conditions

2.7. Modelling of staged construction

For each phase of construction of the structure (change in cross section and load bearing system, prestressing, etc.) its spatial geometry and stiffness is modelled, and the stress-strain state is calculated in all materials for the loads and actions in the phase under consideration. This state is adopted as an initial state for the subsequent phase in which new load bearing elements and new load values are encountered. Thus, in each bridge construction phase, its current stiffness and displacements are

modelled, i.e. the current stress-strain state in the structure is determined and stored.

2.8. Modelling of rheological effects of concrete

A detailed model description is given in [11] and its shorter presentation is given below.

Creep

The Glanville and Dischinger method is used for the calculation of uniaxial strain by creep. The method is based on the assumption that the creep rate is a function of the current uniaxial stress of concrete and time t elapsed after the loading, i.e.

$$\frac{d\varepsilon_t^c}{dt} = f(\sigma, t) \tag{12}$$

If the time is divided into discrete time intervals Δt, with $t_n = t$ i $t_{n+1} = t + \Delta t$, then the incremental version of equation (12) assumes the following form

$$\Delta\varepsilon_{t_{n+1}}^c = \varepsilon_{t_{n+1}}^m \Delta\Phi_{t_n,t_{n+1}} = \varepsilon_{t_{n+1}}^m \left[\Phi_{t_{n+1}} - \Phi_{t_n}\right] \tag{13}$$

where $\Delta\varepsilon_{t_{n+1}}^c$ denotes an increase in creep strain between times t_n and t_{n+1}, ε_{n+1}^m is the instantaneous mechanical strain of concrete over time t_{n+1} (can be a nonlinear stress functionσ), $\Delta\Phi_{t_n,t_{n+1}}$ is the increase in creep coefficient between times t_n and t_{n+1}, $\Phi_{t_{n+1}}$ is the creep coefficient for time t_{n+1} and Φ_{t_n} is the creep coefficient for time t_n. The increment of creep strain $\Delta\varepsilon_{t_{n+1}}^c$ is calculated based on conditions valid at the beginning of the oncoming time increment t_{n+1}. The values according to [19] are used for creep coefficients, and so the expression (13) can be written as follows

$$\Delta\varepsilon_{t_{n+1}}^c = \varepsilon_{t_{n+1}}^m \Phi_0 \left[\beta_{t_{n+1},t_0}^c - \beta_{t_n,t_0}^c\right] \tag{14}$$

where Φ_0 denotes the basic creep value, while β_{t_{n+1},t_0}^c i β_{t_n,t_0}^c denote coefficients that describe the time of creep under load.

Shrinkage

The uniaxial shrinkage of concrete described in [13] and used in this paper can be expressed as:

$$\varepsilon_t^s = \varepsilon^{s0}\beta_t^s \tag{15}$$

where ε_t^s denotes the uniaxial shrinkage strain over time t, ε^{s0} is the basic shrinkage value, and β_t^s is the coefficient describing the time in which shrinkage takes place. In the scope of an iterative time algorithm, an increase in shrinkage strain $\Delta\varepsilon_{n+1}^s$ between two neighbouring times t_n and t_{n+1} can be determined as follows:

$$d\varepsilon_{n+1}^s = \varepsilon^{s0}\left(\beta_{t_{n+1}}^s - \beta_{t_n}^s\right) \tag{16}$$

where the coefficients $\beta_{t_n}^s$ i $\beta_{t_{n+1}}^s$ correspond to times t_n and t_{n+1}. In the context of the shell problem under consideration, it is assumed that the concrete shrinkage takes place in defined orthogonal directions x, y in the shell plane and, at that, shrinkage strain increments $d\varepsilon_x^s$, $d\varepsilon_y^s$ are calculated for particular directions as shown for the one-dimensional problem.

Ageing

The concrete ageing strain is assumed in an indirect way, by increasing over time the initial elastic modulus and strength of concrete. In fact, current mechanical properties of concrete, i.e. the time "strengthened" material, is taken into account during selection of the σ - ε^m relationship in the considered time t_{n+1}. A schematic presentation of concrete ageing for a uniaxial elastoplastic relationshipσ - ε^m is shown in Figure 8.

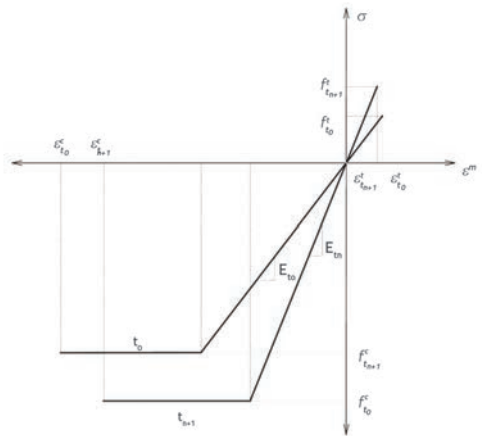

Figure 8. Schematic presentation of concrete ageing for uniaxial elastoplastic relationship σ - ε^m

In Figure 8 t_{n+1} denotes the current time under consideration and t_0 denotes the initial time; f^c stands for the design compressive strength of concrete and f^t denotes the design tensile strength of concrete; E denotes the uniform elastic modulus of concrete in compression and tension; ε^c denotes the design concrete crushing strain in compression and ε^t denotes the design concrete crushing strain in tension. The following is updated in each time step: compressive strength, tensile strength, elastic modulus, and crushing strain. The change in shear modulus of concrete is assumed by the change in elastic modulus. The Poisson ratio is assumed to be invariable over time.

Temperature

If the effect of a known temperature history is considered, then temperature increments are defined in accordance with the time discretisation selected (Figure 9).

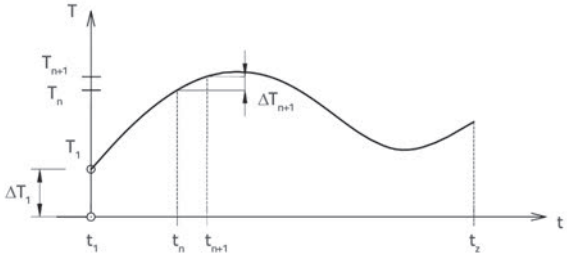

Figure 9. Temperature history

Also, the starting point is the known relationship between the stress vector σ and the vector of mechanical strain of concrete ε^m in each time increment considered, i.e. the known current constitutive model of material which includes the ageing effects (Figure 10).

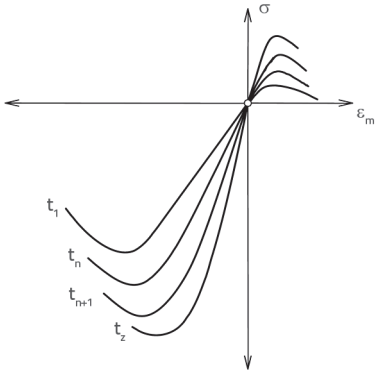

Figure 10. Stress-strain relationship in considered time step (one-dimensional presentation)

2.9. Numerical algorithm for analysis of structure under long-term static loads and actions

The incremental-iterative equilibrium equation for the structure under consideration, corresponding to the current geometry and material characteristics, can be written in the following form [9-11].

$$\mathbf{K}_{n+1}^{i+1}\,\Delta\mathbf{u}_{n+1}^{i+1} = \Delta\mathbf{R}_{n+1} \tag{17}$$

where the index *n* denotes the time increment and *i* stands for the iteration step. $\mathbf{K}_{n+1}^{i+1}$ denotes the tangential stiffness matrix that effect the large displacements. $\Delta\mathbf{u}_{n+1}^{i+1}$ denotes the vector of increase in node displacements, and $\Delta\mathbf{R}_{n+1}$ is the vector of increase of equivalent node forces:

$$\Delta\mathbf{R}_{n+1} = \Delta\mathbf{R}_{n+1}^{e} + \Delta\mathbf{R}_{n+1}^{nm} + \mathbf{R}_{n}^{u} \tag{18}$$

In the above expression $\Delta\mathbf{R}_{n+1}^{nm}$ denotes the vector of increase of external forces, $\Delta\mathbf{R}_{n+1}^{nm}$ is the vector of increase of equivalent node forces due to non-mechanical stran $\Delta\boldsymbol{\varepsilon}_{n+1}^{nm}$ between the times t_{n+1} and t_n (due to creep, shrinkage, ageing, and temperature), and $\Delta\mathbf{R}_{n}^{u}$ stands for unbalanced forces from the preceding time increment *n*. The vector $\Delta\mathbf{R}_{n+1}^{nm}$ can be calculated using the expression

$$\Delta\mathbf{R}_{n+1}^{nm} = \int_V \mathbf{B}_{n+1}^{T}\,\mathbf{D}_{n+1}\,\Delta\boldsymbol{\varepsilon}_{n+1}^{nm}\,dV \tag{19}$$

where $\mathbf{B}_{n+1}^{T}$ denotes the tangent matrix of the displacement-strain relationship, while $\mathbf{D}_{n+1}$ denotes the tangent matrix of the stress-strain relationship. The increment of the total non-mechanical strain $\Delta\boldsymbol{\varepsilon}_{n+1}^{nm}$ is

$$\Delta\boldsymbol{\varepsilon}_{n+1}^{nm} = \Delta\boldsymbol{\varepsilon}_{n+1}^{c} + \Delta\boldsymbol{\varepsilon}_{n+1}^{s} + \Delta\boldsymbol{\varepsilon}_{n+1}^{a} + \Delta\boldsymbol{\varepsilon}_{n+1}^{T} \tag{20}$$

and it is composed of the increment of creep strain $\Delta\boldsymbol{\varepsilon}_{n+1}^{c}$, shrinkage $\Delta\boldsymbol{\varepsilon}_{n+1}^{s}$, ageing $\Delta\boldsymbol{\varepsilon}_{n+1}^{a}$, and temperature changes $\Delta\boldsymbol{\varepsilon}_{n+1}^{T}$.

The total non-mechanical strain is

$$\boldsymbol{\varepsilon}_{n+1}^{nm} = \boldsymbol{\varepsilon}_{n}^{nm} + \Delta\boldsymbol{\varepsilon}_{n+1}^{nm} \tag{21}$$

The increase in total strain $\Delta\boldsymbol{\varepsilon}_{n+1}^{i+1}$ can be calculated as follows

$$\Delta\boldsymbol{\varepsilon}_{n+1}^{i+1} = \mathbf{B}_{n+1}^{i}\,\Delta\mathbf{u}_{n+1}^{i+1} \tag{22}$$

And the total current strain is

$$\boldsymbol{\varepsilon}_{n+1}^{i+1} = \boldsymbol{\varepsilon}_{n+1}^{i} + \Delta\boldsymbol{\varepsilon}_{n+1}^{i+1} \tag{23}$$

The current mechanical strain $\left(\boldsymbol{\varepsilon}^{m}\right)_{n+1}^{i+1}$ is

$$\left(\boldsymbol{\varepsilon}^{m}\right)_{n+1}^{i+1} = \boldsymbol{\varepsilon}_{n+1}^{i+1} - \boldsymbol{\varepsilon}_{n+1}^{nm} \tag{24}$$

The problem solving diagram for the long-term static loads and actions is shown in Figure 11.

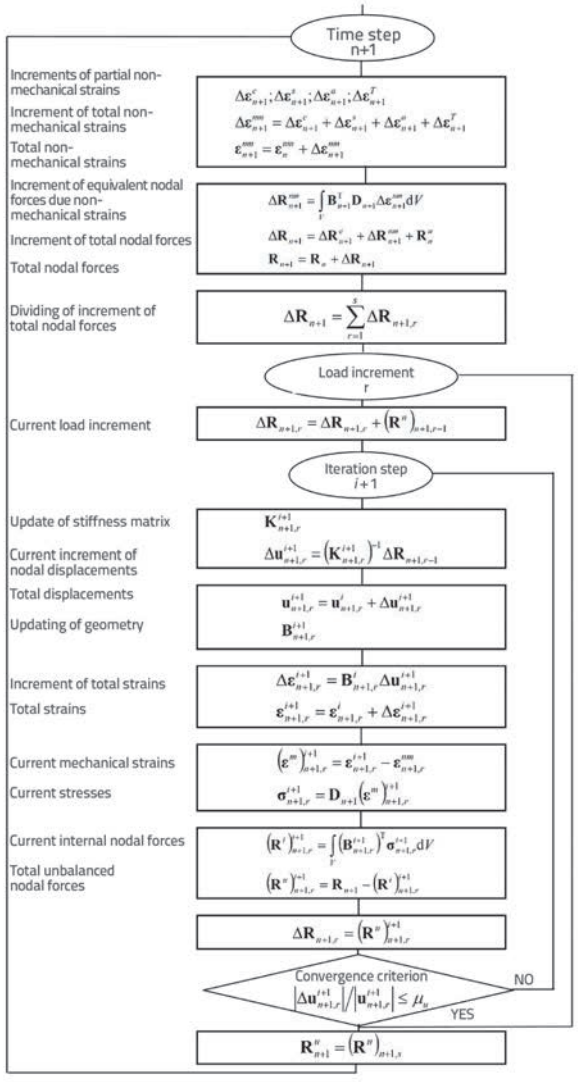

Figure 11. Problem solving diagram for long term loads and actions in incremental-iterative form

2.10. Modelling of prestressing and losses of prestressing force

A detailed description of the model is given in [9-14], and its brief presentation is given below.

2.10.1. Tendon geometry and material model

The tendon geometry is defined with coordinates of points traversed by the tendon axis (Figure 12). The tendon position within the final shell element is shown in Figure 13.

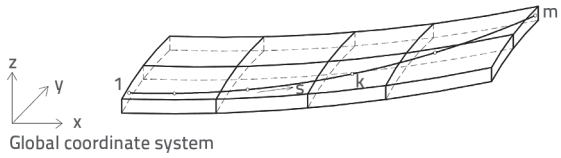

Figure 12. Tendon geometry

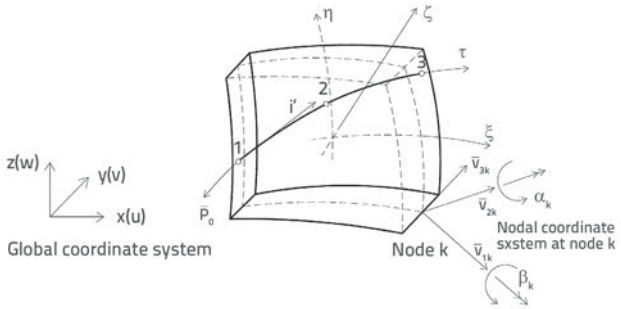

Figure 13. Prestressed tendon embedded in the shell element

In case of pretensioned structures, the unyielding connection is ensured between the concrete and prestressed steel, just like in case of connection between the concrete and reinforcing steel. In case of posttensioned structures, the unyielding connection between the tendon and concrete is ensured only after cable tensioning and grouting, i.e. after grout hardening (the so called bonded tendons).

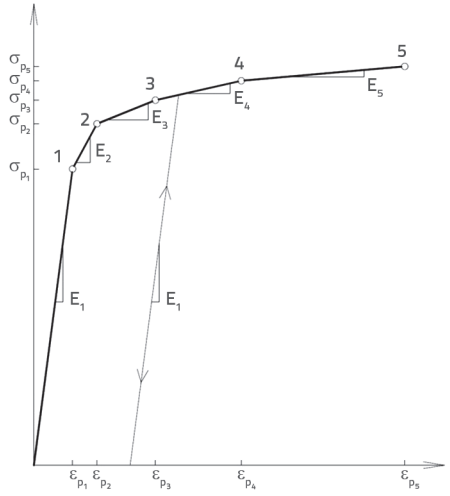

Figure 14. Stress-strain link for prestressed steel

If cables are not grouted, there is no design connection between the concrete and tendon (the so called unbonded tendons). The following steps are required for modelling mechanical effects of the connection between concrete and tendon:

- add contribution of tensioning to the global stiffness,
- calculate strain increase due to tensioning effect, as an external load affecting the structure,
- calculate the final force in tendon and generate internal forces due to tensioning.

The adopted stress-strain relation for prestressed steel is presented in Figure 14.

2.10.2. Modelling of prestressing force losses and force transfer from tendon to concrete

Force losses due to friction and dowel slip are simulated in accordance with [19] (Figure 15). Losses due to relaxation of prestressed steel are modelled according to [20] (Figure 16). Force losses due to instantaneous strain of concrete, and losses due to concrete creep and shrinkage, are automatically included in the model. The prestressing is modelled by the initial tendon strain, which corresponds to the prestressing force. The prestressing force is applied in the system as equivalent nodal forces. Once the equilibrium for prestressing is established, the svstem is solved for other external loads.

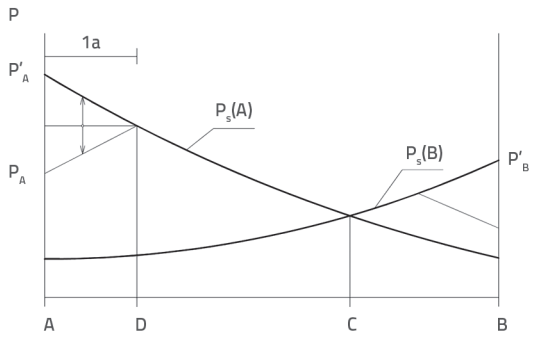

Figure 15. Friction-generated change in prestressing force along tendon

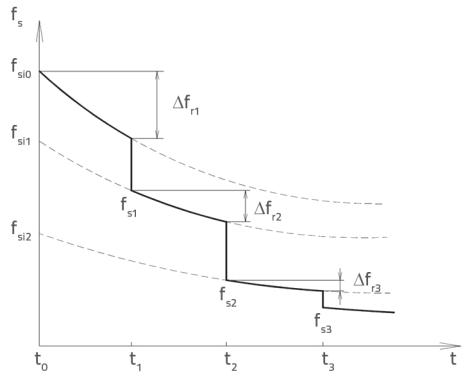

Figure 16. Calculation of initial tendon stress losses at repeated load due to prestressed steel relaxation

2.11. Critical review of adopted assumptions and accuracy of developed numerical model

A numerical model that would describe with complete accuracy the real behaviour of the studied structures, which is obviously highly complex, has not as yet been developed. The objective of the presented model is to provide a sufficiently realistic and technically acceptable simulation of the real behaviour of the considered structures. At the same time the aim is to keep the model relatively simple and adjusted to practical use, i.e. to include the lowest possible number of parameters. Assumptions adopted in the structural material models, and assumptions regarding the geometry of the structure, its construction stages, loads and actions, and design algorithms, are such that the presented numerical model still ensures a very good correspondence with numerous experimental results and results of other numerical models, even for the cases of deep nonlinear behaviours (see references [9-17]). Nevertheless, an additional verification of this model is considered necessary. Further improvements in the accuracy of the model are possible, and some of them are indicated below. These improvements would certainly contribute to its complexity and would involve incorporation of parameters that in most cases can not be accurately defined for analysis of practical structures.

- more adequate concrete modelling in compression, tension, and shear,
- more adequate modelling of rheological properties of concrete, and incorporation of the influence of repeated (cyclical) load for all materials,
- more adequate modelling of tendons and concrete-tendon connection, and change of the force in tendon over time,
- improvement of numerical calculation procedures, etc.

3. Stress ribbon bridge over the Cetina River at Zadvarje

The Cetina River has an up to 150 m deep and steeply carved riverbed in its lower reaches, in the immediate vicinity of Zadvarje, approximately 15 km upstream from Omiš. At this locality, the Cetina Canyon is amazingly beautiful and attractive, quite favourable for white-water rafting, climbing and other extreme sports. The natural beauty of the landscape is further emphasized by magnificent Velika and Mala Gubavica waterfalls, storming down with an incredible noise onto the riverbed approximately 60 m below. Every visitor will certainly remain trilled by this unique and wildly romantic spectacle.

In the scope of its tourist development plans, the Zadvarje municipality hopes to benefit from the European funding and build at the Gubavica Waterfall locality a pedestrian and bicycle bridge, which would also link the Cetina banks and contribute to the development of the wider region.

The bridge would be located about 85 m to the downstream of the waterfall, in a sound rock zone less influenced by the wind. In this zone, the banks of the river are about 250 m apart at the ground surface level. To reduce the bridge span and wind load, i.e. to reduce its price and obtain a spectacular view of the waterfalls, the bridge grade is lowered for approximately 15 m with respect to the surrounding terrain level. At this level, the bridge span is considerably reduced.

The bridge solution based on the tension ribbon system (Figure 17) was selected as it presents many advantages compared to other possible alternatives. The bridge is 150 m in span and 3 m in total width, with the sag of f = 6,5 m (f/L = 0,043). A somewhat greater bridge sag was adopted so as to increase the rationality of the solution, and to enable its appropriate use. The deck slab is composed of prefabricated concrete elements, made to act compositely with in situ concrete. At most of the bridge length the deck slab thickness is 26 cm and it increases to 94 cm toward the abutments.

Figure 17. Visualisation of stress-ribbon bridge over the Cetina near Zadvarje

The bridge has four load-bearing tendons, each 2400 mm^2 (16 x 0.6") in area, and eight pretensioned cables. Four pretensioned tendons are 1050 mm^2 (7 x 0.6") in area, two occupy an area of 1800 mm^2 (12 x 0.6"), while the area of the remaining two is 2400 mm^2 (16 x 0.6"). This pretensioning is to be made in two phases: one and seven days after construction of the monolithic bridge. The area of the prefabricated concrete cross-section amounts to 0.2276m^2 in span zone, and 0.6332m^2 of the in situ concrete (in span zone). Prefabricated elements are made of concrete class C 55/67, and the in situ concrete class C 40/50. The traditional longitudinal reinforcement of the in situ concrete is about 1 % of the concrete cross-section area. Bridge abutments are relatively small concrete blocks, each anchored into the stone cliff by 16 anchors measuring 16 x 0.6", with the total force of 16x2190 = 26280 kN. The vertical compressive force of 17017 kN is transferred from the foundations onto the cliff ($\sigma_{tla,rd}$ = 0,8 MPa). Some details of the solution applied in the abutment zone are shown in Figure 19.

Using the numerical model described in Section 2, and the spatial discretisation according to Figure 20 with 1820 shell and 1400 cable elements (with denser distribution near the supports), the bridge was calculated for permanent load and

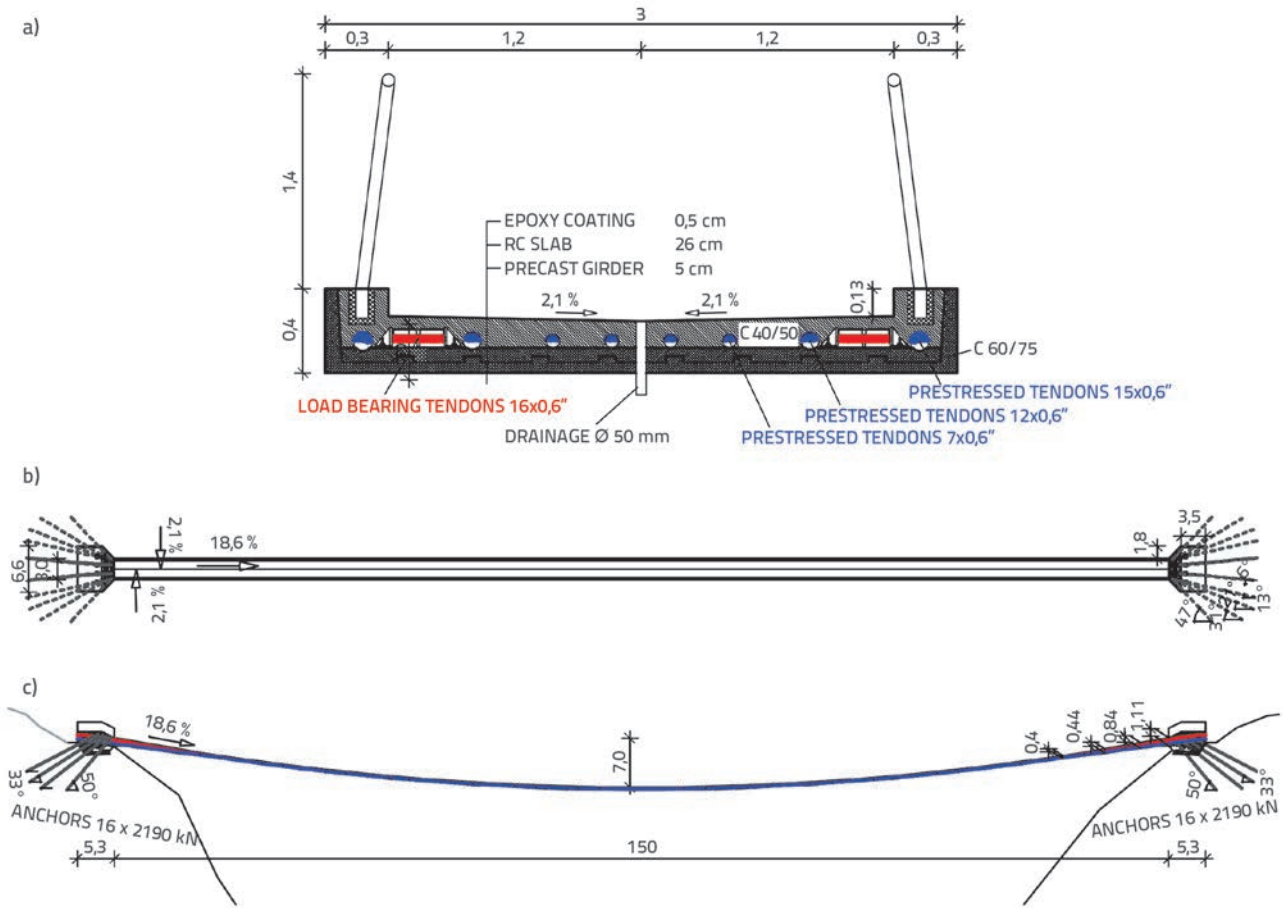

Figure 18. Basic solutions of stress-ribbon bridge over the Cetina at Zadvarje: a) mid-span cross section; b) plan view; c) longitudinal view

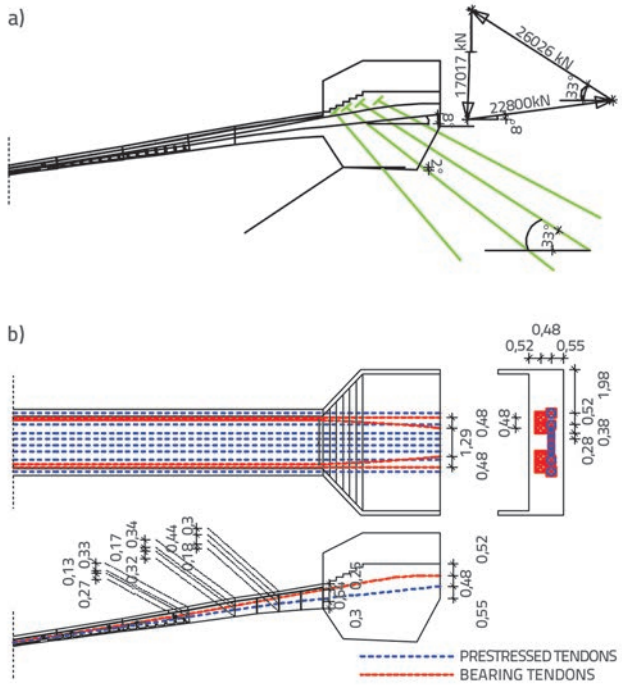

Figure 19. Some bridge solutions at abutments: a) resulting forces in tendons and ground anchors; b) tendon guiding details

actions (self-weight, additional permanent load, prestressing, creep and shrinkage), variable actions (traffic load, temperature actions, and wind load) and seismic actions. Ultimate limit states and serviceability limit states were checked. All calculations were conducted according to prevailing Croatian standards [19, 22-32]. The traffic load of 3 kN/m^2 was adopted (for pedestrian load over the entire bridge span, i.e. 3.5 kN/m^2 for the half-bridge span load). The wind load adopted for pedestrian traffic amounts to W_z=0,4 kN/m^2, W_x=W_y=1,25 kN/m^2. Creep curves obtained from creep test at early loading [33] were used for the first prestressing phase (concrete at one day of age). Creep curves according to [19] were used for the second prestressing phase.

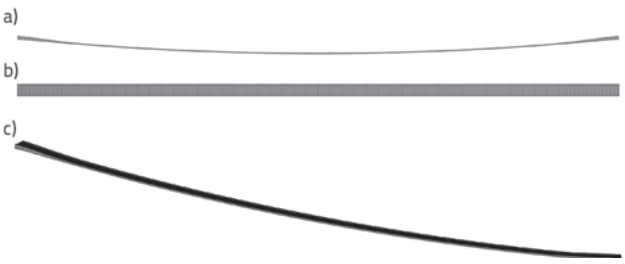

Figure 20. Spatial discretisation of bridge: a) side view; b) plan view; c) spatial view

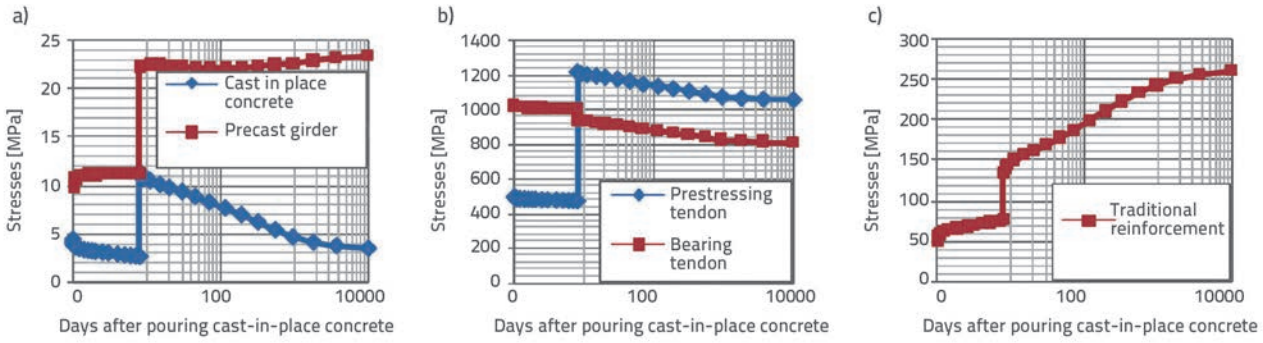

Figure 21. Superstructure stresses in mid-span of the bridge for quasi-permanent load: a) concrete structure; b) steel tendons; c) traditional reinforcement

Table 2. Deflections and stresses in mid-span of the bridge for some loads over various time intervals

Days / Deflections and stresses	0	1	8	8	30	30	30	10000	10000	10000
Phases [loading]	Construction	1st pretensioning phase	Before 2nd pretensioning phase	After 2nd pretensioning phase	Quasi-static load	SLS	ULS	Quasi-static load	SLS	ULS
Deflection in mid-span of the bridge [m]	7.00	6.85	6.77	6.60	6.49	6.56	6.67	6.20	6.30	6.55
Stresses in load-bearing tendons [MPa]	1074	1026	1001	948	911	933	965	811	840	911
Stresses in pretensioned tendons [MPa]		494	470	1214	1172	1194	1226	1052	1081	1152
Stresses in cast in situ concrete [MPa]		-4.5	-2.7	-11.4	-9.4	-5.2	0.0	-3.5	0.0	0.0
Stresses in prefabricated concrete [MPa]		-9.9	-11.3	-22.3	-22.4	-17.7	-10.9	-23.4	-17.2	-1.9
Stresses in traditional reinforcement [MPa]		-51.4	-77.4	-134.6	-170.0	-146.5	-112.5	-260.4	-229.4	-152.5

GSU - combination for serviceability limit state = $1{,}0 \cdot G + 1{,}0 \cdot P + 1{,}0 \cdot Q + 0{,}6 \cdot T_{-25}$
GSN - combination for ultimate limit state = $1{,}35 \cdot G + 0{,}9 \cdot P + 1{,}5 \cdot Q + 0{,}9 \cdot T_{-25}$
Quasi-permanent combination = $1{,}0 \cdot G + 1{,}0 \cdot P + 0{,}2 \cdot Q + 0{,}5 \cdot T_{-25}$ [shrinkage and creep are included in the model]
Q - Pedestrians over the entire bridge

A number of combinations of relevant loads and actions are analysed (permanent load, prestressing, three cases of pedestrian load, four cases of wind load, three cases of temperature action, and the shrinkage, creep and ageing of concrete over time), including construction in stages, with combination coefficients according to [19]. Only some calculation results are presented in the paper. Figure 21 shows stresses in individual parts of the structure in the mid-span of the bridge for quasi-permanent load ($1{,}0 \cdot G + 1{,}0 \cdot P + 0{,}5 \cdot T_{-25}$ + shrinkage and creep). Deflection and stresses in the mid-span of the bridge are presented in Table 2 for some loads expressed in time intervals.

The ultimate limit state is relevant when the bridge is put to use (thirtieth day after construction) as the stresses in tendons and concrete are then the greatest. The serviceability limit

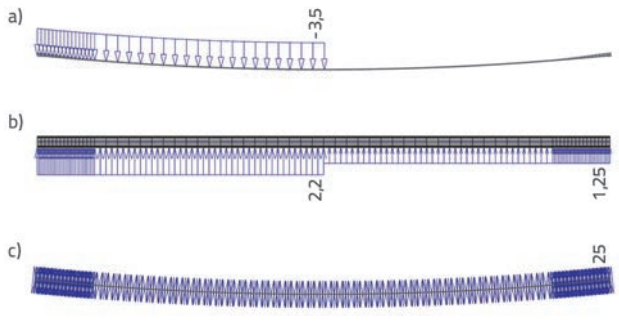

Figure 22. Some loads in serviceability combination K1 (permanent load is automatically included, while prestressing is simulated by initial deformation); a) $Q_{0,5}$ – pedestrian load over one half span (kN/m²); b) $W_{0,5}$ - corresponding wind load for $Q_{0,5}$ (kN/m); c) ΔT^{+} uniform increase in temperature (°C)

state (checking cracks in concrete) is relevant after most of the rheological effects have been realized (ten thousand days after construction) as the level of the prestress in concrete is then the smallest. The age of ten thousand days is taken as the limit in which over 95% of long-term effects are presumed to have been realized. Some calculation results for the serviceability combination K1 (Figure 22), K1= $1,0 \cdot G + 1,0 \cdot P + 1,0 \cdot Q_{0,5} + 0,6 \cdot \Delta T_{+} + 0,3 \cdot W_{0,5}$, are presented in Figure 23.

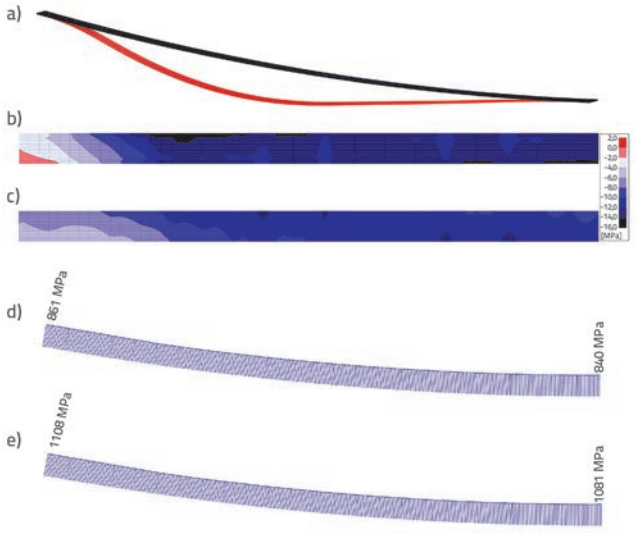

Figure 23. Some calculation results for serviceability combination of load K1: a) displacements – spatial view; b) longitudinal stresses at top edge of the bridge – presented at mid-span of the bridge; c) longitudinal stresses at bottom edge of the bridge – presented at mid-span of the bridge; d) stresses in load bearing tendons – presented at mid-span of the bridge; e) stresses in pretensioning tendons – presented at mid-span of the bridge

An earthquake is not relevant for calculation of this bridge. Some free bridge-oscillation modes and the corresponding oscillation periods are presented in Figure 24.

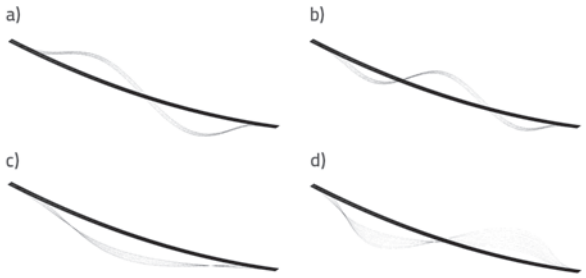

Slika 24. Some free oscillation modes for the bridge: a) first mode, T_1 = 3,71 s; b) second mode, T_2 = 2,56 s; c) third mode, T_3 = 1,72 s; d) eighth mode - torsional, T_8 = 0,62 s

4. Conclusion

Stress-ribbon bridges deserve a much wider application in practice because of their rationality, rapid construction, favourable appearance, harmonious blending in with the environment, and small maintenance costs. Reliable analyses of such bridges require definition of influences with respect to the change in their geometry, change in cross-section and superstructure bearing system during construction, nonlinear behaviour of materials, pretensioning, rheological effects of materials, etc. The developed numerical model for the analysis of stress-ribbon bridges under the short-term (static and dynamic) and long-term loads and actions can simulate all main nonlinear effects relating to the behaviour of these structures. The model is relatively simple and is based on basic material-related parameters. It has already been checked on several occasions, and was successfully implemented in the design of the stress-ribbon bridge over the Cetina River at Zadvarje. The proposed bridge solution is considered both appropriate and rational. The developed numerical model and the corresponding computer software for the calculation of stress-ribbon bridges need further verification.

REFERENCES

[1] Strasky, J.: *Stress Ribbon and Cable-Supported Pedestrian Bridges*, Thomas Telford Publishing, London, 2005., http://dx.doi.org/10.1680/sracspb.32828

[2] Kalafatić, I., Radić, J., Šavor, Z.: Proračun prednapetih provješenih mostova, *Građevinar 61* (2009) 9, pp. 827-836.

[3] Japan Prestressed Concrete Engineering Association: *Standard of Design and Construction of Stress-Ribbon Bridge* (Draft), Japan, 2000.

[4] Newland, D. E.: Pedestrian Excitation of Bridges, *Journal of Mechanical Engineering Science 218* (2004) 5, pp. 477-492.

[5] Markocki, B., Salamak, M.: Durability of Stress Ribbon Bridge Checked during Loading Test, *Journal of Civil Engineering and Architecture 8* (2014) 4, pp. 470-476.

[6] Caetano, E., Cunha, A.: Experimental and Numerical Assessment of the Dynamic Behaviour of a Stress-Ribbon Footbridge, *Journal of Structural Concrete 5* (2004) 1, pp. 29-38.

[7] Toskhiko A., Kiyoshi U., Yoshio F., Hiroshi O., Masakatsu W.: Dynamic Characteristic and Earthquake Response Analysis of Three-Span Continuous Stress Ribbon Bridge, *12th World Conference on Earthquake Engineering*, Auckland, New Zealand, 2000.

[8] Bleicher, A., Schlaich, M., Fujino, Y., Schauer, T.: Model-Based Design and Experimental Validation of Active Vibration Control for a Stress Ribbon Bridge Using Pneumatic Muscle Actuators, *Engineering structures 33* (2011) 8, pp. 2237-2247.

[9] Radnić, J., Matešan, D., Harapin, A.: Model for Static Analyses of Concrete Shell, *Engineering Modelling 13* (2000) 3-4, pp. 93-99.

[10] Radnić, J., Harapin, A., Matešan, D.: Statička i dinamička analiza betonskih ljusaka, *Građevinar 53* (2001) 11, pp. 695-709.

[11] Radnić, J., Matešan, D.: Proračun betonskih ljusaka s uključenjem reoloških svojstava betona, *Građevinar 55* (2003) 1, pp. 1-13.

[12] Radnić, J., Matešan, D.: Experimental Testing of RC Slab Behaviour under Long-Term Load, *Materialwissenschaft und Werkstofftechnik 39* (2008), pp. 157-161, http://dx.doi.org/10.1002/mawe.200700261

[13] Radnić, J., Matešan, D.: Analiza prednapetih betonskih ljusaka pod dugotrajnim opterećenjem, *Građevinar 62* (2010), pp. 183-196.

[14] Matešan, D., Radnić, J.: Nonlinear Time-Dependent Analysis of Prestressed Concrete Shells (Chapter), *Materials with complex behaviour*, (Eds. Öchsner, A. et al.), Springer-Verlag, Berlin (2010), pp. 165-179.

[15] Radnić, J., Matešan, D.: Testing of Prestressed Concrete Shell under Long-Term Loading and Unloading, *Experimental Mechanics 50* (2010), pp. 575-588, http://dx.doi.org/10.1007/s11340-009-9242-9

[16] Matešan, D., Radnić, J., Baloević, G., Smilović, M.: Nonlinear Analysis of Concrete Shells Including Effects of Normal and Transverse Shear Stresses, *Materialwissenschaft und Werkstofftechnik 45* (2014) 4, pp. 258-268.

[17] Radnić, J., Matešan, D., Grgić, N., Baloević, G.: Impact testing of RC slabs strenghthened with CFRP strips, *Composite Structures 121* (2015) 4-5, pp. 330-347.

[18] Hughes, T.J.R., Liu, W.K.: Nonlinear Finite Element Analysis of Shells: Parts I and II: Three Dimensional and Two Dimensional Shells, *Computer Methods in Applied Mechanics and Engineering 26* (1981), pp. 331-362, *27* (1981), pp.167-181.

[19] HRN EN 1992-1-1:2013, Eurokod 2: Projektiranje betonskih konstrukcija – Dio 1-1: Osnove i pravila primjene za zgrade, Hrvatski zavod za norme, Zagreb, 2013.

[20] Magura, D., Sozen, M. A., Siess, C. P.: A study of stress relaxation in prestressing reinforcement, *PCI Journal 9* (1964) 2: pp. 13-57.

[21] Buklijaš-Kobojević, D.: Projekt pješačkog mosta u Zadvarju, diplomski rad (mentor Radnić, J.), Split, 2013.

[22] HRN EN 1992-1-1:2013/NA:2013, Eurokod 2: Projektiranje betonskih konstrukcija – Dio 1-1: Osnove i pravila primjene za zgrade - Nacionalni dodatak, Hrvatski zavod za norme, Zagreb, 2013.

[23] HRN EN 1992-2:2013, Eurokod 2: Projektiranje betonskih konstrukcija – Dio 2: Betonski mostovi - Proračun i pravila razrade detalja, Hrvatski zavod za norme, Zagreb, 2013.

[24] HRN EN 1992-2:2013/NA:2013, Eurokod 2: Projektiranje betonskih konstrukcija – Dio 2: Betonski mostovi - Proračun i pravila razrade detalja - Nacionalni dodatak, Hrvatski zavod za norme, Zagreb, 2013.

[25] HRN EN 1990:2011, Eurokod 0: Osnove projektiranja konstrukcija, Hrvatski zavod za norme, Zagreb, 2011.

[26] HRN EN 1990:2011, Eurokod 0: Osnove projektiranja konstrukcija - Nacionalni dodatak, Hrvatski zavod za norme, Zagreb, 2011.

[27] HRN EN 1991-1-4:2012, Eurokod 1: Djelovanja na konstrukcije – Dio 1-4: Opća djelovanja - Djelovanja vjetra, Hrvatski zavod za norme, Zagreb, 2012.

[28] HRN EN 1991-1-4:2012/NA:2012, Eurokod 1: Djelovanja na konstrukcije – Dio 1-4: Opća djelovanja - Djelovanja vjetra - Nacionalni dodatak, Hrvatski zavod za norme, Zagreb, 2012.

[29] HRN EN 1991-2:2012, Eurokod 1: Djelovanja na konstrukcije – Dio 2: Prometna opterećenja mostova, Hrvatski zavod za norme, Zagreb, 2012.

[30] HRN EN 1991-2:2012/NA:2012, Eurokod 1: Djelovanja na konstrukcije – Dio 2: Prometna opterećenja mostova - Nacionalni dodatak, Hrvatski zavod za norme, Zagreb, 2012.

[31] HRN EN 1997-1:2012, Eurokod 7: Geotehničko projektiranje – Dio 1: Opća pravila, Hrvatski zavod za norme, Zagreb, 2012.

[32] HRN EN 1997-1:2012/A1:2014, Eurokod 7: Geotehničko projektiranje – Dio 1: Opća pravila, Hrvatski zavod za norme, Zagreb, 2012.

[33] Atrushi, D. S.: *Tensile and Compressive Creep of Early Age Concrete: Testing and Modelling* (PhD thesis), Department of Civil Engineering, The Norwegian University of Science and Technology, Trondheim, Norway, 2003.